

Hot-carrier thermal breakdown and S-type current-voltage characteristics in perforated graphene structures

V. Ryzhii^{1,2*}, C. Tang^{1,2}, M. Ryzhii³, and M. S. Shur⁴

¹Frontier Research Institute for Interdisciplinary Sciences, Tohoku University, Sendai 980-8578, Japan

²Research Institute of Electrical Communication, Tohoku University, Sendai 980-8577, Japan

³School of Computer Science and Engineering, University of Aizu, Aizu-Wakamatsu 965-8580, Japan

⁴Department of Electrical, Computer, and Systems Engineering, Rensselaer Polytechnic Institute, Troy, New York 12180, USA

*Author to whom correspondence should be addressed: vryzhii@gmail.com

We investigate the carrier transport characteristics of perforated graphene layer (PGL) composed of arrays of interdigital coplanar graphene microribbons (GMRs) connected by graphene nanoribbon (GNR) bridges. We analyze their operation at room-temperature. Under an applied bias voltage, two-dimensional electron and hole systems (2DES and 2DHS) form in adjacent GMRs. The terminal current in these PGL structures is primarily governed by thermionic transport across the GNR bridges. As electrons and holes traverse the GNRs, they induce heating in the 2DES and 2DHS, creating a positive feedback loop between carrier heating and thermionic emission. This phenomenon, characterized as hot-carrier thermal breakdown, can give rise to S-shaped inter-GMR current-voltage characteristics. These unique transport properties make PGLs promising candidates for fast, voltage-controlled room-temperature switches and electromagnetic radiation detectors.

Remarkable properties of graphene layers (GLs), enable their use in detectors, amplifiers, and sources of the terahertz radiation,^{1–17} as well as optoelectronic devices,^{18–20} and other systems based on graphene micro- and nanoribbons (GMRs and GNRs) and hybrid structures.^{21–28} The graphene-based topological structures using GL-GMR-GNR arrays presents new opportunities for enhancing the performance of graphene devices. Recently, GMR-GNR terahertz photomixers and detectors based on in-plane interdigital GMR-GNR arrays, where GNR bridges connect adjacent GMRs to form inter-GMR barriers through bandgap opening,^{29–31} have been proposed and evaluated.^{32,33} Such or similar device structures can be fabricated on the perforated graphene layers (PGLs) with the GNRs bridges connecting the GNRs. The energy barriers in the inter-perforation constrictions depend on the perforation shape and carrier transport across the GNR bridges can occur via tunneling, thermally-assisted tunneling, or thermionic mechanisms. The dominant transport mechanism is critical for the operation of different devices with the GNR bridges. In constrictions with variable width characterized by fairly smooth barriers (such as parabolic barriers), the energy barriers are relatively smooth. In such cases, the thermionic mechanism can play a significant role even at large band openings (2Δ), provided that the terminal voltage V_G is sufficiently high.

In this paper, we consider the transport in the PGLs featuring interdigital coplanar GMRs connected by the GNR bridges of nearly parabolic form. These PGLs can exhibit interesting features the occurrence of the hot-carrier thermal breakdown leading to the S-shaped dependences of the electron and hole effective temperature T and the terminal current J on the bias voltage V_G (the $T - V_G$ and $J - V_G$ characteristics). Notably, the proposed PGLs can serve as fast voltage-pulse-controlled current switches operating at room tempera-

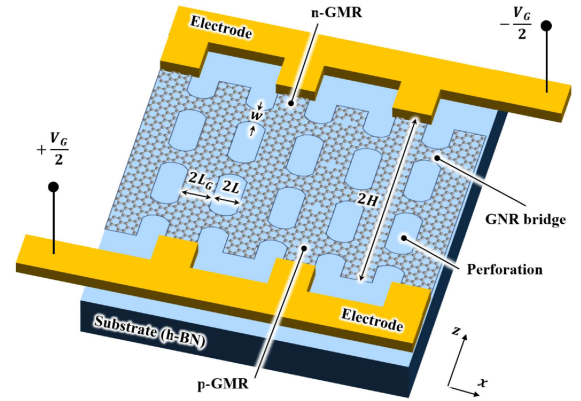


FIG. 1. Schematic top view of the PGL device structure.

ture.

Figure 1 shows the PGL structure under consideration. This structure is an array of the interdigital strips (i.e., GMRs) connected by GNRs bridges. The opposite ends of the interdigital GMRs are connected to the corresponding poles of the bias voltage source. The terminal voltage V_G (applied to the ends of the neighboring GMRs) induces the electron and hole charges, i.e., the two-dimensional electron and hole systems (2DESs and 2DHSs), in the neighboring GMRs. Therefore the n-GMR and p-GMRs alternate. The PGL structures are assumed to be placed on substrates, such as the hexagonal-BN substrates or embedded in the layers of this material. Figures 2 presents the band diagram at the PGL structure at the cross-sections corresponding to the GNRs under the applied voltage V_G . We assume that the minimal thickness of the GNRs is chosen to be sufficiently small to provide a reasonable band gap opening due to quantization of the electron and hole spec-

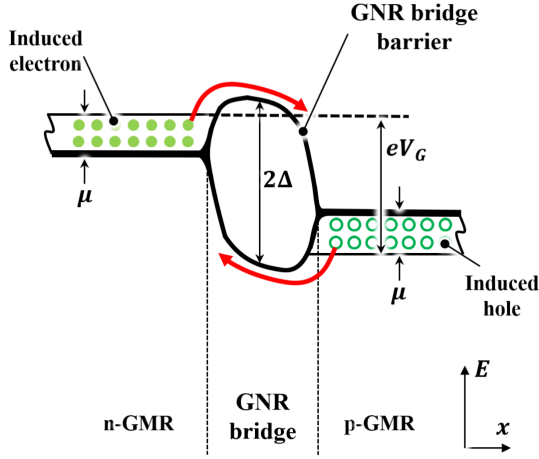


FIG. 2. The PGL band diagram for one structure period at cross-sections corresponding to GNRs.

tra. The number, $2N - 1$, of the CNR bridges between each pair of the GMRs may vary, provided it satisfies the condition $(2N - 1W) \ll 2H$, where $2H$ is the GMR length. The GNR width $2L$ should be sufficiently large to prevent the quantum coupling of the electrons and holes in adjacent GNRs. These constraints imply that the inter-GMR conductance (through all the GNRs) remains much smaller than the conductance along the GMRs. This assumes that the energy barriers for the electrons and holes in the perforations between the GNRs are sufficiently large, being small compared with the energy barriers in the perforations (determined by the GMR/h-BN band offsets). As a result, the electrons and holes incident on these barriers are reflected (at least at moderate voltages), so that the inter-GMR currents through the perforations are suppressed. Consequently, the electron and hole currents between the neighboring GMRs flow through the GNR bridges.

The GMR number, $2M$, can vary from two ($M = 1$, i.e., one n-GMR and one p-GMR) to a large number ($M \gg 1$). Apart from the applied voltage V_G , the electrically induced electron and hole densities, depend on the inter-GMR capacitance c_G ,^{34,35} which, in turn, is determined by the GMR width $2L_G$ and the inter-GMR spacing equal to $2L$ (see Fig. 1). Due to the in-plane configuration, the inter-GMR capacitance c_G can be much smaller than the capacitance of the gated GMRs (as in the field-effect transistors). The capacitance smallness is beneficial for enhancing the speed of the PGL-based devices.

The height of the barriers in the GNR bridges (limiting the electron and hole current through them), formed due to the electron and hole transverse confinement in the GNR and, hence, the quantization of the electron and hole spectra is estimated as $\Delta = \pi\hbar v_W/w$. Here w is the GNR minimal width ($w < W$ or even $w \ll W$), $v_W \simeq 10^8$ cm/s is the carrier velocity in GLs, and \hbar is the Planck constant. We assume that the GNR width $W(x)$ (with $W(x)|_{x=0} = w$) corresponds to the parabolic form of the energy barrier $\Delta(x)$, such that $\Delta(x)|_{x=\pm L} = 0$ and $\Delta(x)|_{x=0} = \Delta$.

Following the Landauer-Buttiker formula³⁶ (see also, for

example, Refs.³⁷⁻³⁹) applied to the one-dimensional transport through the GNRs, the current, $j_{GMR} = j_{GMR}(z)$, of the electrons and holes via one GNR, forming a near-parabolic energy barrier, at the net voltage V_G between its ends, can be approximated by the following extrapolation:

$$j_{GMR} \simeq \frac{8eT}{\pi\hbar} \exp\left(\frac{\mu - \Delta}{T}\right) \sinh\left(\frac{eV_G}{2T}\right). \quad (1)$$

Here $\mu = e\sqrt{\bar{V}_G V_G}$ is the electron and hole Fermi energy in the pertinent GMRs induced the bias voltage with the characteristic voltage $\bar{V}_G = (\pi c_G \hbar^2 v_W^2 / 2e^3 L_G)$, where $c_G = [(\kappa_S + 1)/4\pi^2] \bar{c}_G$ is the inter-GMR capacitance, κ_S is the substrate dielectric constant, and \bar{c}_G is a function of the L_G/L ratio.

The injected carriers transfer the energy $\delta\varepsilon = eV_G$ per carrier to the respective GMR. Considering this, the carrier effective temperature T , can be determined by balancing the energy received by the 2DES and 2DHS in the GMRs due to the injection of the hot carriers, and the energy dissipated to the lattice and the side contacts. Hence, the carrier energy balance in the GMRs is governed by the following equation:

$$4MHL_G \Sigma_{GR} = JV_G. \quad (2)$$

Here $\Sigma_G = c_G V_G / e$ is the GMR carrier density induced by the bias voltage and $J = M(2N - 1)j_{GMR}$ is the net terminal current. The quantity Σ_{GR} is the rate of carrier energy relaxation in the GMRs per unit of their area. We focus on the PGL at room temperature, when the carrier energy relaxation on optical phonons is a crucial mechanism (see, Refs. 39-55). However, at the high carrier temperatures comparable to or higher than the optical phonon energy in GMRs $\hbar\omega_0 \simeq 0.2$ eV, the rate of energy relaxation due to optical phonon mechanism (OP mechanism) saturates becoming unable to compensate the carrier heating associated with the hot carrier injection (see below). This implies that at elevated carrier temperature other energy relaxation mechanism can be essential. Due to this, apart from the optical phonon scattering mechanism (the OP mechanism), we include in our model the energy relaxation

| | |
|--|---------------------------|
| GMR length, $2H$ | (0.5 - 1.0) μm |
| GNR length, $2L$ | 40 nm |
| GMR width, $2L_G$ | 60 nm |
| GNR minimal width, w | (6 - 12) nm |
| GNR barrier height, Δ | (150 - 300) meV |
| Substrate dielectric constant, κ_S | 10 |
| GMR-GNR capacitance, c_G | 0.576 |
| Characteristic voltage, \bar{V}_G | 8 meV |
| Number of GNR bridges, $(2N - 1)$ | 1 and 5 |
| Lattice temperature, T_0 | 25 meV |
| Optical phonons energy, $\hbar\omega_0$ | 200 meV |
| OP energy relaxation time, τ_0^e | 20 ps |
| SC energy relaxation parameter, S | 10 |
| Carrier momentum relaxation frequency, ν | 1 and 3 ps ⁻¹ |

TABLE I. Main device parameters

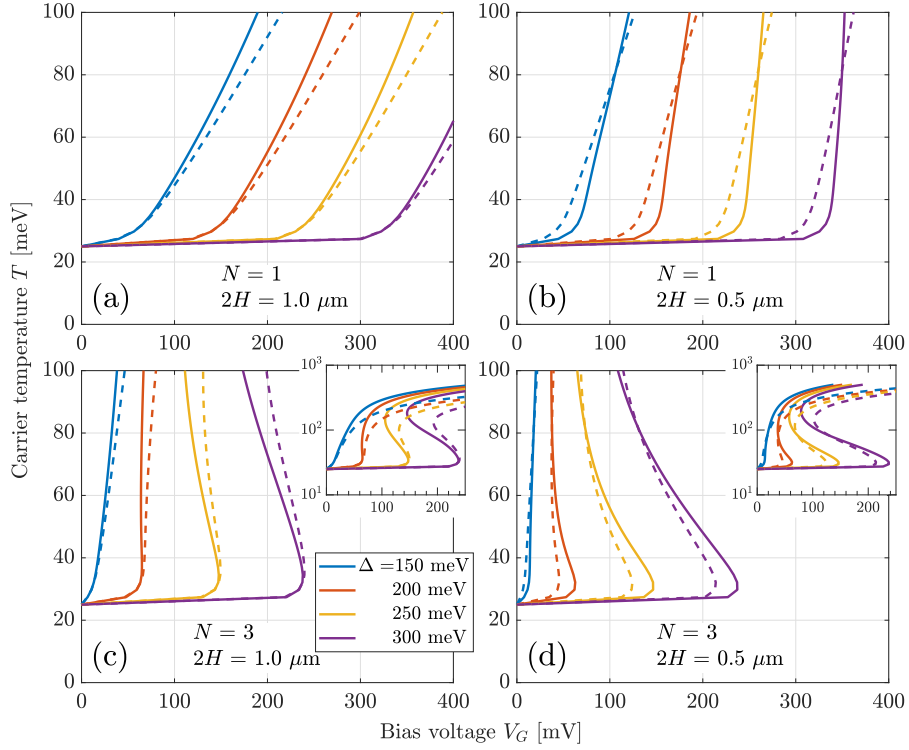


FIG. 3. The $T - V_G$ dependences for devices with different structural parameters for the carrier collision frequency $\nu = 1 \text{ ps}^{-1}$ - solid lines and $\nu = 3 \text{ ps}^{-1}$ - dashed lines, respectively. The insets show the same dependences as in (c) and (d) in a wider temperature range (in the logarithmic scale).

mechanisms associated with the supercollisions and the plasmonic interactions⁵⁶⁻⁵⁸ (the SC mechanism) and the mechanism associated with the transmission of the carrier heat to the side contact and their cooling at the contact (CC mechanism),⁵⁹⁻⁶². As a result, the energy balance is described by the following equation (compare with Refs. 10 and 54):

$$R \simeq \frac{\hbar\omega_0}{\tau_0^\varepsilon} \left(\frac{T_0}{\hbar\omega_0} \right)^2 \left[\exp\left(\frac{\hbar\omega_0}{T_0} - \frac{\hbar\omega_0}{T} \right) - 1 \right] + \frac{1}{\tau_S^\varepsilon} \frac{(T^3 - T_0^3)}{3T_0^2} + \frac{(T - T_0)}{\tau_C^\varepsilon}. \quad (3)$$

Here $\tau_0^\varepsilon = \tau_0(T_0/\hbar\omega_0)^2 \exp(\hbar\omega_0/T_0)$, $\tau_S^\varepsilon = S/\nu$, and $\tau_C^\varepsilon = 2\nu(2H)/v_W^2$ are the "warm" carrier energy relaxation times (i.e., at $T \simeq T_0$) due to the OP, SC, and CC mechanisms, respectively, τ_0 is the characteristic time of the spontaneous optical phonon emission, ν is the carrier collision frequency on acoustic phonons, impurities, and due to carrier viscosity effects⁶³, with $S > 1$ being considered as the fitting parameter). At $T \simeq T_0$, Eq. (3) yields $R \simeq (T - T_0)/\tau^\varepsilon$ with $1/\tau^\varepsilon = 1/\tau_0^\varepsilon + 1/\tau_S^\varepsilon + 1/\tau_C^\varepsilon$.

Equations (1), (3), and (4) lead to the following equations parametrically relating J and V_G via T as a parameter:

$$J \simeq J_M \left[\exp\left(\frac{\hbar\omega_0}{T_0} - \frac{\hbar\omega_0}{T} \right) - 1 + \frac{(T^3 - T_0^3)}{T_0^3} K_S + \frac{(T - T_0)}{T_0} K_C \right] \quad (4)$$

and

$$V_G = \frac{\bar{V}_G}{4} \left[\sqrt{1 + \frac{4B(T)}{e\bar{V}_G}} - 1 \right]^2. \quad (5)$$

The solution of coupled Eqs. (5) and (6) yields the $T - V_G$ and $J - V_G$ characteristics. The function $B(T)$ in Eq. (6) is given by

$$B(T) = 2T \sinh^{-1} \left\{ \frac{T_0}{2T\Theta_N} \exp\left(\frac{\Delta}{T} \right) \times \left[\exp\left(\frac{\hbar\omega_0}{T_0} - \frac{\hbar\omega_0}{T} \right) - 1 + \frac{(T^3 - T_0^3)}{T_0^3} K_S + \frac{T - T_0}{T_0} K_C \right] \right\}. \quad (6)$$

Above $J_M = (4MH_C T_0)/e\tau_0^\varepsilon (T_0/\hbar\omega_0)$ is the characteristic current, $K_S = (\tau_0^\varepsilon/3\tau_S^\varepsilon)(\hbar\omega_0/T_0)$ and $K_C = (\tau_0^\varepsilon/\tau_C^\varepsilon)(\hbar\omega_0/T_0)$ describe the relative contribution of the energy relaxation mechanisms under consideration, and $\Theta_N = (2N - 1)[2\tau_0^\varepsilon e^2/\pi\hbar H_C G](\hbar\omega_0/T_0)$.

At not too large voltages when $\sqrt{\bar{V}_G}, V_G < T_0/e$ the carrier effective temperature only slightly exceeds the lattice temperature, i.e., $T \gtrsim T_0$. In this case, Eqs. (4) - (6) yield¹¹

$$J \simeq 4M(2N - 1) \left(\frac{e^2}{\pi\hbar} \right) \exp\left(-\frac{\Delta}{T_0} \right) V_G. \quad (7)$$

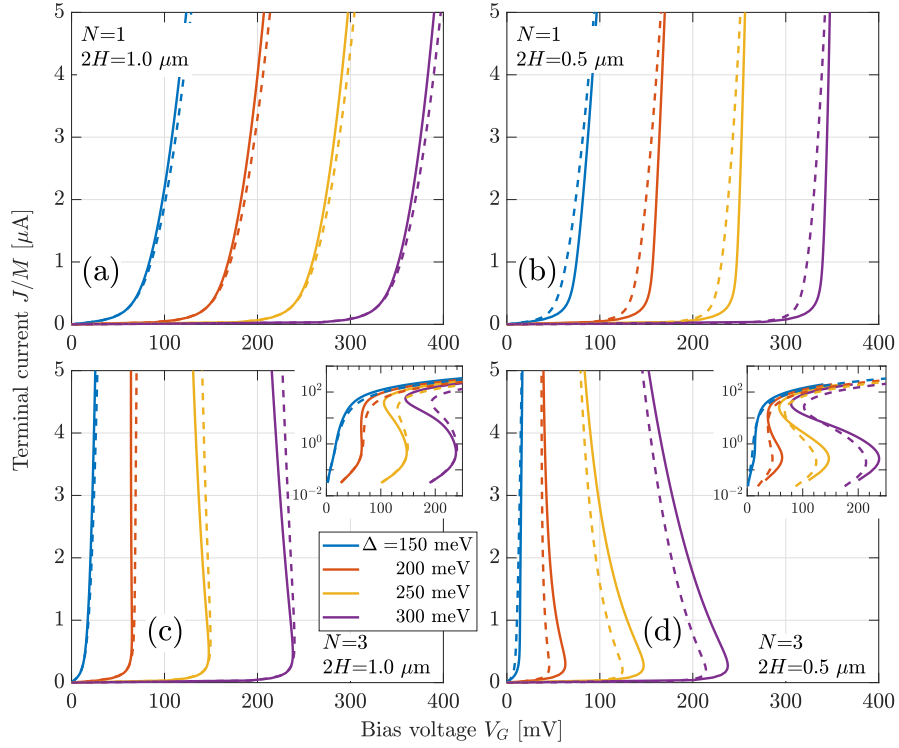


FIG. 4. The terminal current J (normalized by the number, M , of GMR pairs) versus bias voltage V_G for the $T - V_G$ dependences in Fig. 3: $\nu = 1 \text{ ps}^{-1}$ - solid lines and $\nu = 3 \text{ ps}^{-1}$ - dashed lines. REPLACE H by $2H \text{ nm}$

Further increase in the terminal voltage leads to a steep rise of the carrier temperature and the terminal current. It is interesting that when parameter Θ_N is sufficiently large (there are several GNR bridges between the GMRs and the GMR length $2H$ is not too long), the derivative dT/dV_G turns to infinity at certain threshold voltage \bar{V}_N^{th} , which corresponds to the threshold temperature \bar{T}_N^{th} . According to Eq. (4), the differential conductance $dJ/dV_G \propto dT/dV_G$, dJ/dV_G also turns to infinity at the same threshold voltage \bar{V}_N^{th} . As follows from Eqs. (5) and (6), the threshold voltage \bar{V}_N^{th} exists if the parameter $\Theta_N \propto (2N - 1)/H$ is sufficiently large, exceeding a certain critical value Θ .

Beyond the voltage threshold, an increase in the effective temperature and the current can not be limited by the OP energy relaxation mechanism. This phenomenon can be referred to as the hot-carrier thermal breakdown. In this case, the $T - V_G$ and $J - V_G$ characteristics can be ambiguous

In such a situation, the rise of T and J at $V_G > \bar{V}_N^{th}$ is stopped by the inclusion of the SC and CC mechanisms, which are effective at elevated carrier temperatures, so that the $T - V_G$ and $J - V_G$ characteristics shape becomes S-type.

Figures 3 and 4 show the $T - V_G$ and $J - V_G$ characteristics obtained using the above equation for the PGL structures with different numbers of the GNR bridges ($2N - 1$), different GMR length $2H$, different values of the GNR energy barrier Δ , and collision frequency ν . Table I lists the device parameters used in the calculations.

One can see from Figs. 3(a) and 3(b) that in the structures with a single GNR bridge [$(2N - 1) = 1$ and $H = 1.0 \text{ } \mu\text{m}$ and $H = 0.5 \text{ } \mu\text{m}$] corresponding to relatively small $\Theta_1 < \Theta$ ($\Theta_1 \simeq 140$ and 280 , respectively), the $T - V_G$ characteristics are monotonous. A decrease in H and, hence, an increase in Θ_1 leads to steeper $T - V_G$ characteristics. This is because in shorter GMRs the total number of the carriers $\propto H$ heated by the inter-GMR current is smaller at the same injected current.

In contrast, in the case of several GNR bridges [for example, at $(2N - 1) = 5$ as shown in Figs. 3(c) and 3(d) with $\Theta_3 > \Theta$], the $T - V_G$ dependences become ambiguous. These dependences are characterized by the threshold voltages \bar{V}_3^{th} in the range $50 - 220 \text{ mV}$ (for the assumed structural parameters). It is instructive that the pertinent values of the threshold temperatures ($\bar{T}_3^{th} \simeq 33 \text{ meV}$) only moderately exceed the lattice temperature T_0 . This implies that in such structures the $J - V_G$ threshold can occur at relatively weak carrier overheating. The inclusion of the SC and CC energy relaxation mechanisms results in higher branches of the $T - V_G$ and $J - V_G$ characteristics leading to the S-shape of these characteristics [see the insets in Figs. 3(c) and 3(d) and in Figs. 4(c) and 4(d)]. The shapes of the $T - V_G$ and $J - V_G$ characteristics shown in Figs. 3 and 4 are similar. The upper branches of these characteristics are characterized by their threshold voltages $\tilde{V}_N^{th} < \bar{V}_N^{th}$. The difference $\bar{V}_N^{th} - \tilde{V}_N^{th}$ increases with increasing Θ_N and Δ .

As seen from the comparison of the plots corresponding to different collision frequency (the solid and dashed lines in

Figs. 3 and 4), the characteristics variations are rather small. This is attributed to a relatively weak role of the SC and CC mechanisms except in the high voltage/high temperature ranges, at least at the chosen PGL parameters (their contribution depends on ν). Thus, the thermal breakdown and the S-type characteristics can occur at a large number of the GNR bridges and short GMRs. It is crucial that in the PGLs under consideration with the identical energy barriers for the electrons injected from the n-GMR and holes injected from p-GNRs, the pertinent injected currents are bound by the positive feedback: the electron injection leads to heating of the 2DHS reinforcing the hole injection and vice versa. One needs to stress that the similarity of the electron and hole injection properties is crucial for realizing the positive feedback in question and the the PGL S-type characteristics.

For the values of parameters corresponding to the S-type $J - V_G$ characteristics, the PGL can exhibit two stable current states with the positive differential conductance if $\tilde{V}_N^{th} < V_G < \bar{V}_N^{th}$ - low and high current states, \bar{J} and \tilde{J} , respectively. In the PGLs with the parameters corresponding to Fig. 4(c) and 4(d), $(\bar{J} - \tilde{J})/M \sim 100 \mu\text{A}$.

The switching between these state can be realized by voltage pulses with the opposite polarity and the amplitude $\Delta V_G > (\bar{V}_N^{th} - V_G), (V_G - \tilde{V}_N^{th})$. The switching time is determined by the processes of the carrier heating and cooling, which are characterized by the room temperature effective energy relaxation time τ^e being in the range of 10 - 50 ps.

In conclusion, we analyzed carrier heating in PGLs and demonstrated that it can induce hot-carrier thermal breakdown, leading to the S-shaped current-voltage characteristics. This effect arises from the positive feedback between thermionic currents—flowing between neighboring GMRs via GNR bridges—and carrier heating. The unique characteristics of PGLs can enable fast, voltage-controlled current switches operating at room temperature. Furthermore, the features of the PGL characteristics make these structures promising for applications such as radiation detectors.

The authors are grateful to Prof. T. Otsuji for long-time productive collaboration. The work was supported by JST ALCA-NEXT (Grant No.24021835), NEDO (Grant No.20020912), Murata Foundation (Grant No.AN24322) Iketani Foundation (Grant No.0361181-A), ROHM Co. Ltd, and SCAT Foundation, Japan, the work at RPI was funded by AFOSR (Contract No. FA9550-19-1-0355). USA.

AUTHOR DECLARATIONS

The authors have no conflicts to declare.

DATA AVAILABILITY

The data that support the findings of this study are available within the article.

REFERENCES

- ¹F. Xia, T. Mueller, Y. Lin, A. Valdes-Garcia, and P. Avouris, "Ultrafast graphene photodetector," *Nat. Nanotechnol.* **4**, 839 (2009).
- ²V. Ryzhii, M. Ryzhii, V. Mitin, and T. Otsuji, "Terahertz and infrared photodetection using p-i-n multiple-graphene-layer structures," *J. Appl. Phys.* **107**, 054512 (2010).
- ³L. Vicarelli, M.S. Vitiello, D. Coquillat, A. Lombardo, A.C. Ferrari, W. Knap, M. Polini, V. Pellegrini, and A. Tredicucci, "Graphene field-effect transistors as room-temperature terahertz detectors," *Nat. Mater.* **11**, 865 (2012).
- ⁴V. Ryzhii, M. Ryzhii, M. S. Shur, V. Mitin, A. Satou, and T Otsuji, "Resonant plasmonic terahertz detection in graphene split-gate field-effect transistors with lateral p-n junctions," *J. Phys. D: Appl. Phys.* **49**, 315103 (2016). Perforated gated (induced p-i-n), gated capacitance+ quantum,
- ⁵D. A. Bandurin, D. Svintsov, I. Gayduchenko, S. G. Xu, A. Principi, M. Moskotin, I. Tretyakov, D. Yagodkin, S. Zhukov, T. Taniguchi, K. Watanabe, et al. Fedorov, "Resonant terahertz detection using graphene plasmons," *Nat. Comm.* **9**, 5392 (2018).
- ⁶A. Rogalski, "Graphene-based materials in the infrared and terahertz detector families: a tutorial," *Advances in Optics and Photonics* **11**, 314 (2019).
- ⁷V. Ryzhii, M. Ryzhii, D. S. Ponomarev, V. G. Leiman, V. Mitin, M. S. Shur, and T. Otsuji, "Negative photoconductivity and hot-carrier bolometric detection of terahertz radiation in graphene-phosphorene hybrid structures," *J. Appl. Phys.* **125**, 151608 (2019).
- ⁸J. Liu, X. Li, R. Jiang, K. Yang, J. Zhao, S. A. Khan, J. He, P. Liu, J. Zhu, and B. Zeng, "Recent progress in the development of graphene detector for terahertz detection," *Sensors* **21**, 4987 (2021).
- ⁹V. Ryzhii, M. Ryzhii, T. Otsuji, V. Leiman, V. Mitin, and M. S. Shur, "Modulation characteristics of uncooled graphene photodetectors," *J. Appl. Phys.* **129**, 214503 (2021).
- ¹⁰K. Tamura, C. Tang, D. Ogiura, K. Suwa, H. Fukidome, Y. Takida, H. Minamide, T. Suemitsu, T. Otsuji, and A. Satou, "Fast and sensitive terahertz detection with an epitaxial graphene asymmetric dual-grating-gate field-effect transistor structure," *APL Photonics* **7**, 126101 (2022).
- ¹¹Y. Wei, Z. Bao, H. Wu, Y. Zhang, Y. Wen, Z. Hu, X. Pan, S. Lan, L. Zhang, L. Wang, and X. Chen, "High-performance terahertz photodetection in 2D materials and topological materials," *J. Physics D: Applied Physics* **58**, 073002 (2024).
- ¹²J. M. Caridad, O. Castello, S. M. Lopez Baptista, T. Taniguchi, K. Watanabe, H. G. Roskos, and J. A. Delgado-Notario, "Room-temperature plasmon-assisted resonant THz detection in single-layer graphene transistors," *Nano Lett.* **24**, 935 (2024).
- ¹³Q. Wei, W. Zhu, T. Li, B. Song, C. Shi, Y. Qu, H. Yang, J. Zhang, X. Liu, and H. Liu, "Recent advancements in two-dimensional materials for terahertz photodetectors," *Sci China Mat.* **17** Feb, (2025).
- ¹⁴V. Ryzhii, M. Ryzhii, V. Mitin, and T. Otsuji, "Toward the creation of terahertz graphene injection laser," *J. Appl. Phys.* **110**, 094503 (2011).
- ¹⁵V. Ryzhii, T. Otsuji, M. Ryzhii, A. A. Dubinov, V. Ya. Aleshkin, V. E. Karasik, and M. S. Shur, "Negative terahertz conductivity and amplification of surface plasmons in graphene-black phosphorus injection laser heterostructures," *Phys. Rev. B* **100**, 115436 (2019)
- ¹⁶S. Boubanga-Tombet, W. Knap, D. Yadav, A. Satou, D. B. But, V. V. Popov, I. V. Gorbenko, V. Kachorovskii, and T. Otsuji, "Room-temperature amplification of terahertz radiation by grating-gate graphene structures," *Phys. Rev. X* **10**, 031004 (2020).
- ¹⁷T. Otsuji, S. A. Boubanga-Tombet, A. Satou, D. Yadav, H. Fukidome, T. Watanabe, T. Suemitsu, A. A. Dubinov, V. V. Popov, W. Knap, et al. "Graphene-based plasmonic metamaterial for terahertz laser transistors," *Nanophotonics* **11**, 1677 (2022).
- ¹⁸L. Ren, C. L. Pint, L. G. Booshehri, W. D. Rice, X. Wang, D. J. Hilton, K. Takeya, I. Kawayama, M. Tonouchi, R. H. Hauge, and J. Kono, "Carbon nanotube terahertz polarizer," *Nano Lett.* **9**, 2610 (2009).
- ¹⁹M. Liu, X. Yin, and X. Zhang, "Double-layer graphene optical modulator," *Nano Lett.* **12**, 1482 (2012).
- ²⁰V. Ryzhii, M. Ryzhii, T. Otsuji, V. Leiman, S. O. Yurchenko, V. Mitin, and M. S. Shur, "Effect of plasma resonances on dynamic characteristics of double graphene-layer optical modulators," *J. Appl. Phys.* **112**, 104507 (2012).

- ²¹Z. Chen, A. Narita, and K. Müllen, “Graphene nanoribbons: On-surface synthesis and integration into electronic devices,” *Adv. Mat.* **32**, 2001893 (2020).
- ²²Y. Zhai, Y. Xiang, W. Yuan, G. Chen, J. Shi, G. Liang, Z. Wen, and Y. Wu, “Fabrication of graphene nanomesh FET terahertz detector,” *Micro-machines (Basel)* **12**, 641 (2021)
- ²³V. Ryzhii, M. Ryzhii, D. Svintsov, V. Leiman, P. P. Maltsev, D. S. Ponomarev, V. Mitin, M. S. Shur, and T. Otsuji “Real-space-transfer mechanism of negative differential conductivity in gated graphene-phosphorene hybrid structures: Phenomenological heating model,” *J. Appl. Phys.* **124**, 114501 (2018).
- ²⁴V. Ryzhii, M. Ryzhii, D. S. Ponomarev, V. G. Leiman, V. Mitin, M. S. Shur, and T. Otsuji, “Negative photoconductivity and hot-carrier bolometric detection of terahertz radiation in graphene-phosphorene hybrid structures,” *J. Appl. Phys.* **125**, 151608 (2019).
- ²⁵V. Ryzhii, M. Ryzhii, A. Satou, T. Otsuji, V. Mitin, and M.S. Shur, “Effect of Coulomb carrier drag and terahertz plasma instability in p+-p-i-n+ graphene tunneling transistor structures,” *Phys. Rev. Appl.* **16**, 064053 (2021).
- ²⁶J. A. Delgado-Notario, W. Knap, V. Clericò, J. Salvador-Sánchez, J. Calvo-Gallego, T. Taniguchi, K. Watanabe, T. Otsuji, V. V. Popov, D. V. Fateev, et al. “Enhanced terahertz detection of multigate graphene nanostructures,” *Nanophotonics* **11**, 519 (2022).
- ²⁷A. J. Jumaah, H. G. Roskos, and S. Al-Daffaie, “Novel antenna-coupled terahertz photodetector with graphene nanoelectrodes,” *APL Photon.* **8**, 026103 (2023).
- ²⁸V. Ryzhii, C. Tang, T. Otsuji, M. Ryzhii, and M. S. Shur, “Terahertz plasmonic resonances in coplanar graphene nanoribbon structures,” *J. Appl. Phys.* **135**, 114503 (2024).
- ²⁹Y. Son, M. L. Cohen, and S. G. Louie, “Energy gaps in graphene nanoribbons,” *Phys. Rev. Lett* **97**, 216803 (2006).
- ³⁰M. Y. Han and P. Kim, “Graphene nanoribbon devices at high bias,” *Nano Convergence* **1**, 1 (2014).
- ³¹J. Guan and L. Xu, “Energy gaps in BN/GNRs planar heterostructure,” *Materials* **14**, 5079 (2021).
- ³²V. Ryzhii, M. Ryzhii, C. Tang, T. Otsuji, and M. S. Shur, “Resonant plasmonic terahertz photomixing using interdigital graphene micro-nanoribbon arrays,” *Appl. Phys. Lett.* **124**, 163504 (2024).
- ³³V. Ryzhii, C. Tang, T. Otsuji, M. Ryzhii, and M. S. Shur, “Detection of terahertz radiation using topological graphene micro-nanoribbon structures with transverse plasmonic resonant cavities,” *J. Appl. Phys.* **136**, 194502 (2024).
- ³⁴A. Sh. Achoyan, A. E. Yesayan, E. M. Kazaryan, and S. G. Petrosyan, “Two-dimensional p-n junction under equilibrium conditions,” *Semiconductors* **36**, 903 (2002).
- ³⁵O. G. Vendik, S. P. Zubko, and M. A. Nikol’skii, “Modeling and calculation of the capacitance of a planar capacitor containing a ferroelectric thin film,” *Tech. Phys.* **44**, 349 (1999).
- ³⁶M. Buttiker, Y. Imry, R. Landayer, and S. Pinhas, “Generalized many-channel conductance formula with application to small rings,” *Phys. Rev. B* **31**, 6207 (1985).
- ³⁷K. A. Matveev and L. I. Glazman, “Coulomb blockade of activated conduction,” *Phys. Rev. B* **54**, 10339 (1996).
- ³⁸G. Liang, N. Neophytou, D. E. Nikonov, and M. S. Lundstrom, “Performance projections for ballistic graphene nanoribbon field-effect transistors,” *IEEE Trans. Electron Devices* **54**, 677 (2007).
- ³⁹V. Ryzhii, T. Otsuji, M. Ryzhii, N. Ryabova, S. O. Yurchenko, V. Mitin, and M. S. Shur, “Graphene terahertz uncooled bolometers,” *J. Phys. D: Appl. Phys.* **46**, 065102 (2013).
- ⁴⁰F. T. Vasko and V. Ryzhii, “Voltage and temperature dependences of conductivity in gated graphene heterostructures,” *Phys. Rev. B* **76**, 233404 (2007).
- ⁴¹E. H. Hwang and S. Das Sarma, “Acoustic phonon scattering limited carrier mobility in two-dimensional extrinsic graphene,” *Phys. Rev. B* **77**, 115449 (2008).
- ⁴²S. Das Sarma, S. Adam, E. H. Hwang, and E. Rossi, “Electronic transport in two-dimensional graphene,” *Rev. Mod. Phys.* **83**, 407 (2011).
- ⁴³T. Fang, A. Konar, H. Xing, and D. Jena, “Mobility in semiconducting graphene nanoribbons: Phonon, impurity, and edge roughness scattering,” *Phys. Rev. B* **78**, 205403 (2008).
- ⁴⁴K. M. Borysenko, J. T. Mullen, E. A. Barry, S. Paul, Y. G. Semenov, J. M. Zavada, M. Buongiorno Nardelli, and K. W. Kim, “First-principles analysis of electron-phonon interactions in graphene,” *Phys. Rev. B* **81**, 121412R (2010).
- ⁴⁵M. Schutt, P. M. Ostrovski, I. V. Gornyi, and A. D. Mirlin, “Coulomb interaction in graphene: Relaxation rates and transport,” *Phys. Rev. B* **83**, 155441 (2010).
- ⁴⁶M. V Fischetti, J. Kim, S. Narayanan, Zh.-Y. Ong, C. Sachs, D. K. Ferry, S. J. Aboud, “Pseudopotential-based studies of electron transport in graphene and graphene nanoribbons,” *J. Phys: Cond. Mat.* **25**, 473202 (2013).
- ⁴⁷L. Wang, I. Meric, P. Y. Huang, Q. Gao, Y. Gao, H. Tran, T. Taniguchi, K. Watanabe, L. M. Campos, D. A. Muller, et al. “One-dimensional electrical contact to a two-dimensional material,” *Science* **342**, 614 (2013).
- ⁴⁸L. Banszerus, M. Schmitz, S. Engels, J. Dauber, M. Oellers, F. Haupt, K. Watanabe, T. Taniguchi, B. Beschoten, and C. Stampfer, “Ultra-high-mobility graphene devices from chemical vapor deposition on reusable copper,” *Sci. Adv.* **1e1500222** (2015).
- ⁴⁹M. Yankowitz, Q. Ma, P. Jarillo-Herrero, and B. J. LeRoy, “Van der Waals heterostructures combining graphene and hexagonal boron nitride,” *Nat. Rev. Phys.* **1**, 112 (2019).
- ⁵⁰D. Vaquero, V. Clericò, M. Schmitz, J. A. Delgado-Notario, A. Martín-Ramos, J. Salvador-Sánchez, C. A. Müller, K. Rubi, K. Watanabe, T. Taniguchi, et al. “Phonon-mediated room-temperature quantum Hall transport in graphene,” *Nat. Comm.* **14**, 318 (2023).
- ⁵¹F. Rana, P. A. George, J. H. Strait, S. Sharavaraman, M. Charasheyhar, and M. G. Spencer, “Carrier recombination and generation rates for intravalley and intervalley phonon scattering in graphene,” *Phys. Rev. B* **79**, 115447 (2009).
- ⁵²H. Wang, J. H. Strait, P. A. George, S. Shivaraman, V. D. Shields, M. Chandrashekar, J. Hwang, F. Rana, M. G. Spencer, C. S. Ruiz-Vargas, and J. Park, “Ultrafast relaxation dynamics of hot optical phonons in graphene,” *Appl. Phys. Lett.* **96**, 081917 (2010).
- ⁵³J. H. Strait, H. Wang, S. Shivaraman, V. Shields, M. Spencer, and F. Rana, “Very slow cooling dynamics of photoexcited carriers in graphene observed by optical-pump terahertz-probe spectroscopy” *Nano Lett.* **11**, 4902 (2011).
- ⁵⁴V. Ryzhii, M. Ryzhii, V. Mitin, A. Satou, and T. Otsuji, “Effect of heating and cooling of photogenerated electron-hole plasma in optically pumped graphene on population inversion,” *Jpn. J. Appl. Phys.* **50**, 094001 (2011).
- ⁵⁵J. M. Iglesias, M. J. Martín, E. Pascual, and R. Rengel, “Hot carrier and hot phonon coupling during ultrafast relaxation of photoexcited electrons in graphene,” *Appl. Phys. Lett.* **108**, 043105 (2016).
- ⁵⁶J. C.W. Song, M. Y. Reizer, and L. S. Levitov, “Disorder-assisted electron-phonon scattering and cooling pathways in graphene,” *Phys. Rev. Lett.* **109**, 106602 (2012).
- ⁵⁷D. K. Ferry, H. Ramamoorthy, J. P. Bird, “Plasmon-mediated energy relaxation in graphene,” *Appl. Phys. Lett.* **107**, 262103 (2015).
- ⁵⁸D. K. Ferry, R. Somphonsane, H. Ramamoorthy, J. P. Bird, “Energy relaxation of hot carriers in graphene via plasmon interaction,” *J. Comput. Electron.* **15**, 144 (2016).
- ⁵⁹J. Weissman, L. E. Anderson, A. V. Talanov, Z. Yan, Y. J. Shin, D. H. Najafabadi, M. Rezaee, X. Feng, D. G. Nocera, T. Taniguchi, et al. “Electronic thermal transport measurement in low-dimensional materials with graphene non-local noise thermometry,” *Nat. Nanotechnol.* **17**, 166 (2022).
- ⁶⁰Y. Kim, C.-H. Park, and N. Marzari, “The electronic thermal conductivity of graphene,” *Nano Lett.* **16**, 2439 (2016).
- ⁶¹V. Ryzhii, C. Tang, T. Otsuji, M. Ryzhii, V. Mitin, and M. S. Shur, “Effect of electron thermal conductivity on resonant plasmonic detection in the metal/black-AsP/graphene FET terahertz hot-electron bolometers” *Phys. Rev. Appl.* **19**, 064033 (2023).
- ⁶²V. Ryzhii, C. Tang, T. Otsuji, M. Ryzhii, V. Mitin, and M. S. Shur, “Dynamic characteristics of terahertz hot-electron graphene FET bolometers: Effect of electron cooling in channel and at side contacts,” *J. Appl. Phys.* **135**, 194502 (2024).
- ⁶³Y. Zhang and M. S. Shur, “Collision dominated, ballistic, and viscous regimes of terahertz plasmonic detection by graphene,” *J. Appl. Phys.* **129**, 053102 (2021).